Available online at www.sciencedirect.com
SCIENCE DIRECT®
Thin Solid Films 450 (2004) 34–41
www.elsevier.com/locate/tsf

Texture, residual stress and structural analysis of thin films using a combined X-ray analysis

L. Lutterotti[a,b,*], D. Chateigner[c], S. Ferrari[d], J. Ricote[e]

[a]*Dipartimento di Ingegneria dei Materiali, Univ. di Trento, I-38050 Trento, Italy*
[b]*Earth and Planetary Science Department, University of California, Berkeley, CA 94720, USA*
[c]*Laboratoire de Cristallographie et Sciences des Matériaux-ISMRA, F-14050 Caen, France*
[d]*Materials and Devices for Microelectronics Laboratory, INFM. Via C. Olivetti 2. I-20041 Agrate Brianza, Milan, Italy*
[e]*Instituto de Ciencia de Materiales de Madrid, CSIC, Cantoblanco, E-28049 Madrid, Spain*

Abstract

Advanced thin films for today's industrial and research needs require highly specialized methodologies for a successful quantitative characterization. In particular, in the case of multilayer and/or unknown phases a global approach is necessary to obtain some or all the required information. A full approach has been developed integrating novel texture and residual stress methodologies with the Rietveld method (Acta Cryst. 22 (1967) 151) (for crystal structure analysis) and it has been coupled with the reflectivity analysis. The complete analysis can be done at once and offers several benefits: the thicknesses obtained from reflectivity can be used to correct the diffraction spectra, the phase analysis help to identify the layers and to determine the electron density profile for reflectivity; quantitative texture is needed for quantitative phase and residual stress analyses; crystal structure determination benefits of the previous. To achieve this result, it was necessary to develop some new methods, especially for texture and residual stresses. So it was possible to integrate them in the Rietveld, full profile fitting of the patterns. The measurement of these spectra required a special reflectometer/diffractometer that combines a thin parallel beam (for reflectivity) and a texture/stress goniometer with a curved large position sensitive detector. This new diffraction/reflectivity X-ray machine has been used to test the combined approach. Several spectra and the reflectivity patterns have been collected at different tilting angles and processed at once by the special software incorporating the aforementioned methodologies. Some analysis examples will be given to show the possibilities offered by the method.

Keywords: Thin films; Texture; Diffraction; X-Ray; Rietveld method; Residual stress; Reflectivity; Multilayer

1. Introduction

Today film technology has greatly improved and from the technological point of view it is now becoming strategic to have the potentialities to correctly characterize both the research and the consumer production. Performances and lifetime of these films depend on several characteristics, from chemical composition, purity to other physical properties like thicknesses, crystal structures, microstructure, grain texture and residual stresses. A complete characterization of a film or multilayer can be a very demanding task and in some cases even not possible by the actual standard techniques due to its complexity. X-Ray diffraction and reflectivity are ideal tools to perform the aforementioned analyses and are normally employed to analyze the physical characteristics of films/multilayer. The principal limitation is that when two characteristics are too strong (like texture and stress, number of phases/layers and texture, or thickness and stresses) the single analysis method fails. In the present work we are proposing an integrated methodology based on ad hoc instrumentation and data collection strategy to overcome most or all of the previous limitations. Some real analysis examples will be also reported to show the potentialities of the approach.

The basic idea is to describe the sample as a set of physical characteristics and using them to fit a set of diffraction and reflectivity spectra obtained at different position of sample inside the instrument goniometer. The physical properties of the sample (layers thickness-

*Corresponding author. Tel.: +39-461-882414; fax: +39-461-881977.
E-mail address: luca.lutterotti@ing.unitn.it (L. Lutterotti).

0040-6090/04/$ - see front matter © 2003 Elsevier B.V. All rights reserved.
doi:10.1016/j.tsf.2003.10.150

es, phase composition, texture, residual stresses, crystal structure and microstructure) are optimized in a framework derived from the so-called Rietveld method [1].

The principal drawback of this integrated analysis is that it requires a powerful diffraction instrument to collect all the required spectra in a reasonable time. Ideally, synchrotron and neutron facilities with spectrometers equipped with large position sensitive, image plates, CCD or energy dispersive detectors can collect the necessary data in a very short time. However, we aim to demonstrate that this kind of analysis is suitable also in normal laboratories using custom diffractometers and it can be especially advantageous in the case of thin film analyses where X-ray diffraction is employed preferentially to neutron diffraction.

2. Theory

The general principles of the Rietveld method are detailed in some very good Refs. [1,2]. We recall here just few general ideas. The method is based on the least squares fitting of a diffraction spectrum. For a spectrum collected at a specific sample orientation (χ,ϕ) the intensity of the point i can be computed as

$$I_i^{\mathrm{calc}}(\chi,\phi) = \mathrm{bkg}_i + I_0 L_{\mathrm{p}}(2\theta_i) A_i(\chi,\phi)$$

$$\sum_{n=1}^{N_{\mathrm{phases}}} f_n \sum_{k=1}^{N_{h\,k\,l}} m_{k;n} |F_{k;n}|^2 S_{k;n}(2\theta_i - 2\theta_{k;n}) P_{k;n}(\chi,\phi) \qquad (1)$$

assuming the presence of a certain number of phases (N_{phases}) and reflections ($N_{h\,k\,l}$). In a normal Rietveld program, for speed reasons the computation order is not exactly as in Eq. (1). Every component of Eq. (1) is expressed in term of optimizable coefficients like atomic positions, background polynomial coefficients, phase volume fractions, peak shape parameters, cell parameters, etc. and this allows the parameters to be refined through a non-linear least squares fitting algorithm.

For the case of a layered sample or thin film, an additional scaling factor that depends on the phase and its location inside a layer should be added in Eq. (1) [3]. Also the absorption factor A must be computed differently and will contain in addition the layer thickness as a parameter.

The texture of a phase enters explicitly in Eq. (1) as a factor changing the intensity of different peaks as a function of their $(h\,k\,l)$ miller indices and orientation angles $(\chi,\ \phi)$. If a sufficient number of spectra at different tilting angles are collected and analyzed, it permits in principle to reconstruct by fitting the entire three-dimensional orientation distribution function (ODF). The orientation distribution function obtained can be used to predict and verify anisotropic macro properties of the sample like elastic modulus, electrical, magnetic or transport properties, etc.

Two completely different strategies can be used to describe the ODF. The first and more common one (even if not the best) is based on the expansion of the function in spherical harmonics [4]. The principal problem of this method arises from the fact that the harmonic expansion degree is limited by the finite number of measured points over the pole figure space and by the presence of possible ghost (artifacts in the ODF). In practice due to the Friedel law of diffraction and the harmonic expansion approximation, more solutions are possible from a given set of data. The implementation of the spherical harmonic functions into the Rietveld method is described in detail by Popa [5].

An alternative method consists of dividing the ODF in a finite number of regular cells [6]. The ODF function is described by a discrete value of the function inside every cell. The texture factors can be computed integrating along all grains with the $h\,k\,l$ reflection plane perpendicular to the scattering vector. As the function is described typically by a big number of values, these cannot be used as least squares parameters to be refined. The WIMV method of Matthies et al. [6] uses a custom strategy and iteration algorithm to obtain the best ODF reproducing the pole figure texture values maximizing the so-called phon (ODF background or minimum value) and the texture sharpness. Indeed the classical WIMV algorithm was optimized for traditional pole figures analysis where regular coverage in the orientation angles (χ,ϕ) is used. Inside the Rietveld method it requires two additional steps: one for the extraction of the pole figures and the second for the interpolation of these texture weights in a regular grid [7]. This gives less than optimal results in the case of very sharp textures or coarse irregular coverage. To overcome this problem a modified algorithm has been derived from WIMV. The new method, E-WIMV (Extended WIMV), can be used with irregular pole figure coverage and include a smoothing properties based on a similar concept to the tube projection of the ADC algorithm [8]. The ODF cell values are computed through an entropy iteration algorithm that includes the reflections weights

$$\mathrm{ODF}^{(i+1)}(g) = \mathrm{ODF}^{(i)}(g) \prod_{m=1}^{M_{h\,k\,l}} \left(\frac{P_{h\,k\,l}(g^{-1}, h_{\mathrm{m}})}{P^{(i)}_{h\,k\,l}(g^{-1}, h_{\mathrm{m}})} \right)^{\lambda_i \frac{w_{hkl}}{M_{hkl}}} \qquad (2)$$

where $M_{h\,k\,l}$ is the number of division points for the discretization of the integral of all the orientations around the scattering vector for the pole figure $h\,k\,l$; the index (i) denotes the i-th iteration and $P^{(i)}_{h\,k\,l}(g^{-1}, h_{\mathrm{m}})$ is the calculated pole figure value from iteration (i) for the reflection of Miller indices $h\,k\,l$. For more details the reader may see the Refs. [6,9]. The reflection weight $w_{h\,k\,l}$ is introduced to take into account the different

accuracy of the more intense less overlapped reflections respect to the small ones and it is computed in analogy to the powder pattern point intensity weights or from the pole figures extraction algorithm.

The peak position of a generic $h\,k\,l$ reflection is computed from the d-spacing value according to the classical Bragg law. The residual stress or strain analysis starts from the idea that the mean d-space observed by diffraction can be different along different directions if residual or applied stress/strain fields are present.

If the sample is also textured the anisotropy of the elastic modulus may lead to complex nonlinear trends of the peak position respect to the off-plane tilting angle. In the Rietveld texture-stress analysis it is quite straightforward to model with good approximation such nonlinearities [10]. The problem is how to compute the strain tensor responsible of the peak shift from the macro (and micro) residual stress tensor. Several theories are available for the elastic case [11], and in the present formulation we have adopted the BulkPathGEO method described by Matthies et al. [12]. It makes use of the same formalism enlightened in the geometrical mean to compute the aggregate elastic properties for a textured sample [13] and it proved to be very accurate. For simplicity we point the reader to the original treatment of the authors.

Reflectivity has been added to the least squares Rietveld refinement using the Matrix formalism [14]. The diffraction spectra and reflectivity pattern can be refined together enabling the accurate refinement of small thicknesses and a suitable correction of the diffraction intensities to obtain more reliable texture values in the global fitting procedure.

All the reported methodologies have been implemented inside the software MAUD [15].

3. Experimental

Three thin film samples have been measured using three different diffractometers.

The first is a film composed by 400 nm of $Pb_{0.76}Ca_{0.24}TiO_3$ (PTCa) deposited by spin coating using a sol–gel solution over a (1 0 0) Si wafer with a 50-nm Pt buffer layer. The diffraction measurements were done at the LPEC laboratory in Le Mans using a closed Eulerian goniometer equipped with a 120° position sensitive detector and a graphite primary monochromator. Full spectra of 120° in 2θ were collected using a regular grid of 5°×5° in χ and ϕ with χ from 0° to 50° and ϕ from 0° to 355°. Each spectrum was collected for 1 min and the Eulerian cradle was set at 16.55° in ω to obtain the more complete pole figure coverage for the interesting PTCa peaks approximately at 33° in 2θ. The (1 1 1) Pt and (1 1 1) PTCa peaks are completely overlapped as many other PTCa reflections making it impossible to obtain a quantitative or even qualitative texture analysis from this system using traditional pole figure analysis.

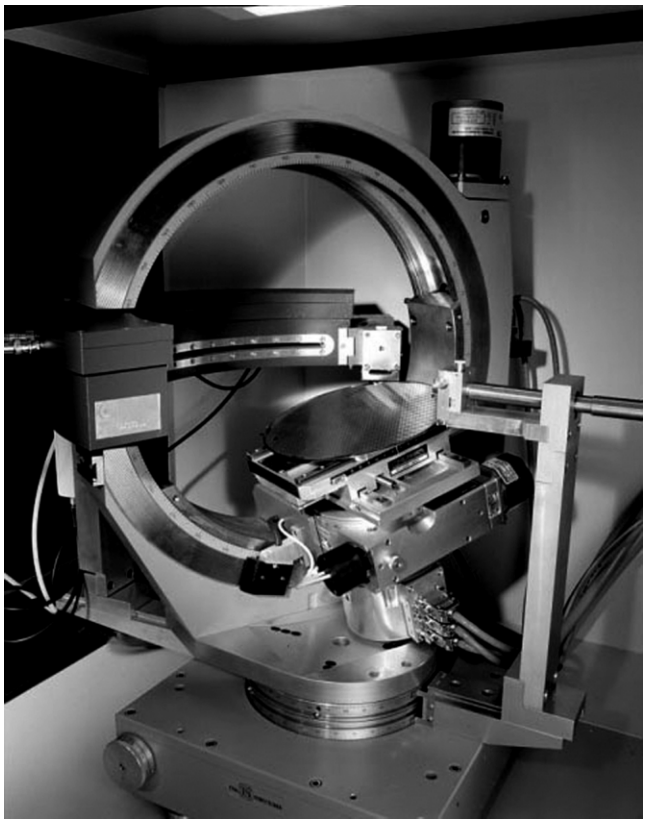

Fig. 1. ESQUI goniometer at the MDM-INFM lab.

The second sample is a cubic Ca stabilized zirconia film deposited by magnetron sputtering over a Si wafer [10]. The sample has been measured using a stress-texture goniometer equipped with a scintillation detector. Spectra were collected in θ–2θ condition from 0° to 50° in χ and at only two different ϕ positions as from a previous preliminary measurement the qualitative texture resulted slightly tetragonal but nearly fiber like. As the detector was a point one, there was the need to reduce the number of spectra as much as possible and still the measurement was taking a full week respect to the day or half day experiments using the position sensitive detector instruments. The data was analyzed with MAUD using E-WIMV and the new BulkPathGEO method described in the theoretical section.

The reflectivity pattern for the third sample, a 20-nm zirconia film, was collected using the ESQUI instrument illustrated in Fig. 1 [16]. With respect to the Le Mans instrument, the Eulerian cradle is open and the primary beam is focused by a multilayer to a parallel very thin beam allowing the measurement of reflectivity patterns also. For this kind of measurement two different measurements modes can be used. One using the position sensitive detector and scanning in θ–2θ at low angle to

collect off-reflectivity patterns, the second mode is more classical and is a normal $\theta-2\theta$ scan using the point detector attached near the position sensitive. This second mode was used for the measurement. Diffraction patterns were subsequently collected with the sample as mounted for reflectivity. The intensity diffracted was very low due to the small thickness of the film, so to reduce the measurement time to reasonable values, only χ tilting were performed spinning the motor ϕ during the measurement to enforce a fiber texture and avoiding collection of spectra at different ϕ.

4. Discussion

The experimental spectra of the PTCa film have been analyzed by the program MAUD [15] in order to test some of the texture models and the layered approach. A starting model has been defined using two layers, one of PTCa over a layer of 50 nm of Pt. To simplify the analysis the Si wafer has been neglected, and the few spectra showing a little Si peak ($\approx 33.5^\circ$ in 2θ) were removed from the refinement.

The first texture model used was the harmonic. It turns out immediately that the texture was sufficiently sharp to require an expansion $L=22$. Using triclinic sample symmetry (equivalent to no symmetry) it requires the refinement of 1245 parameters only for the texture of the PTCa. In reality the texture for this sample is very close to a fiber texture, as it will be confirmed by the direct texture methods (WIMV, E-WIMV), so we imposed fiber symmetry to the sample texture in both the PTCa and Pt (only for the harmonic). This reduced the number of coefficients and consequently parameters in the refinement to a more manageable number.

Fig. 2 reports the fitting result for the E-WIMV texture model that was showing the best agreement with the experimental data. The principal panel shows the experimental and recalculated spectra using the gray color for the intensity. Each spectrum correspond to an ideal horizontal line and from the bottom to nearly half of the panel are reported the experimental data, then there is a small horizontal line of a different (but constant) color that separate the upper part containing the recalculated spectra. The refinement is good when the two, upper and lower, half of the map match closely. The progressive number goes from the first spectrum at $\chi=0^\circ$ and $\phi=0^\circ$ and increases with the angle ϕ until the next χ. The vertical darker strips correspond to the peaks of the two phases. The change in color (intensity) of the strips is due to the strong texture. These vertical lines are also shifting in 2θ and initially this was attributed to residual stresses, but the shifts are bigger at low angle than at high angle, contrary to what is observed for residual stress. In reality the shift is due to the beam not perfectly centered respect to the Eulerian

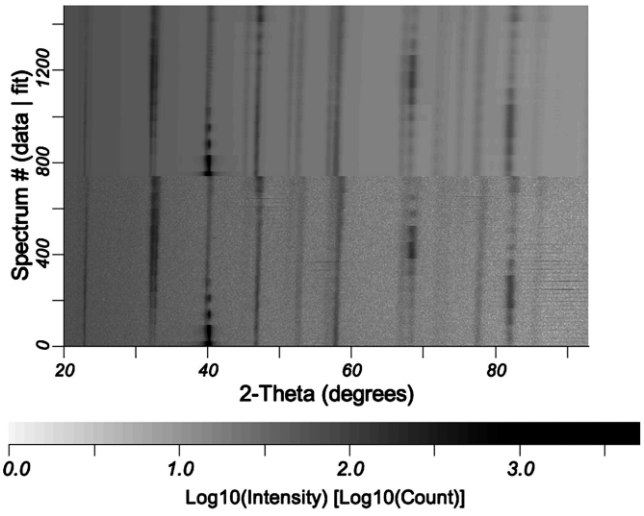

Fig. 2. Plot of the experimental and recalculated diffraction spectra for the PTCa film refined using the E-WIMV texture model. See text for details.

cradle but it was modeled successfully in the refinement. No appreciable residual strain was found.

The reconstructed pole figures for the three texture methods (harmonic, WIMV and E-WIMV) are reported in Fig. 3 for the PTCa and in Fig. 4 for the Pt along with the extracted experimental pole figures. The problem of the harmonic method is visible there, as we can recognize the presence of some negative pole densities, especially for the Pt that shows the stronger texture. These correspond to negative values in the ODF that is physically impossible, thus showing a good example of a ghost problem. The WIMV and E-WIMV methods instead cannot generate negative points due to their algorithm structure as proved in Figs. 3 and 4.

The index of the spectra fitting, R_{WP}, increased a little from 25% with the harmonic to 25.5% using the WIMV. This is mainly due to the fact that the WIMV method is working outside the least squares method and thus the texture is not highly optimized for the spectra fitting. The R_{WP} index dropped down to 19.9% for E-WIMV indicating an even better spectra fitting than the harmonic thanks to the new algorithm that permits to avoid the interpolation step required by WIMV. The E-WIMV in this case gives the best results in term of spectra fitting and ODF reproduction. But in any case the texture analysis is quite similar to the WIMV case; only the ODF results smoother due to the tube projection adoption.

Both WIMV and E-WIMV confirmed the nearly fiber texture of the sample and validate the assumption made for the harmonic analysis. Comparing all the reconstructed pole figures with the experimental ones (extracted from the spectra) of Fig. 3d and Fig. 4d we can clearly see as the harmonic method has more difficulties to

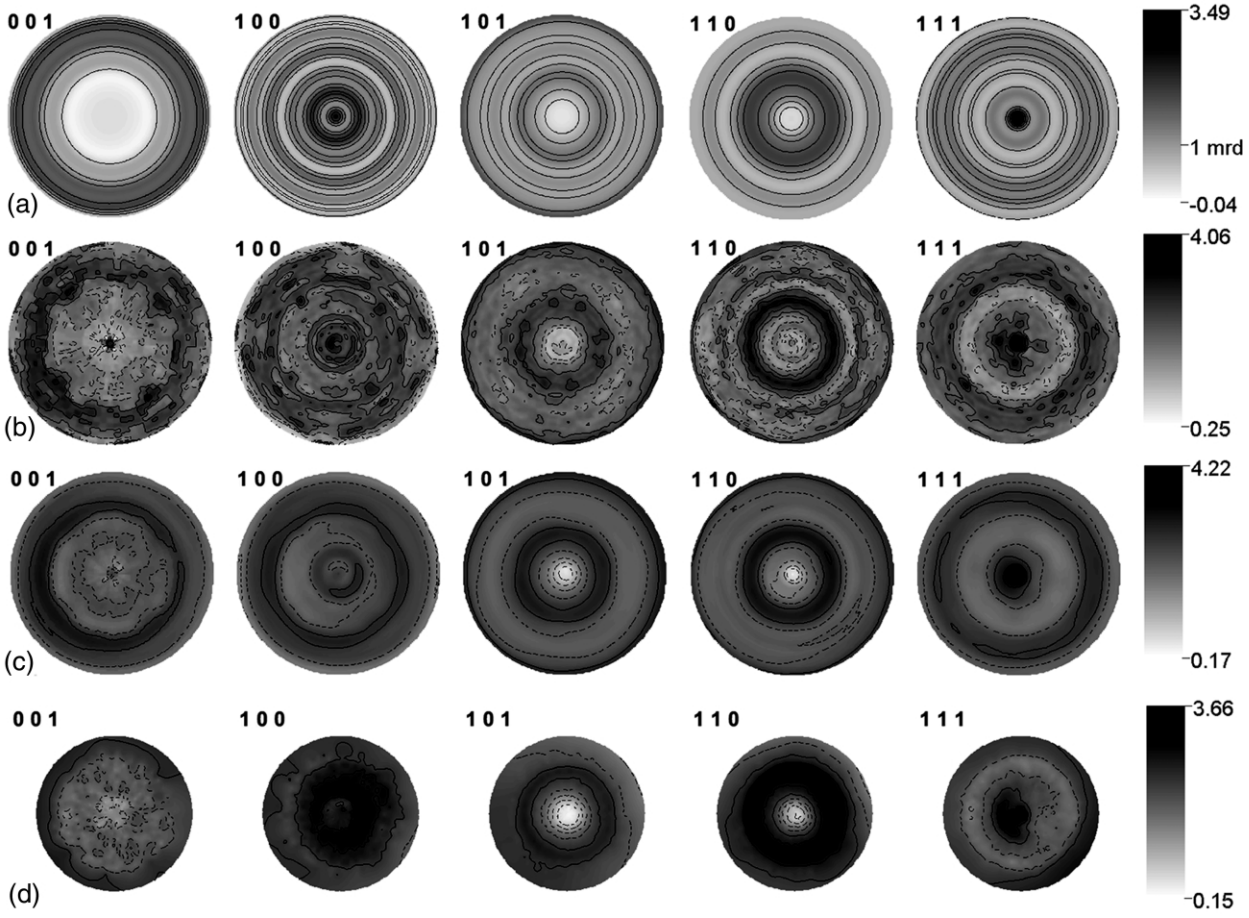

Fig. 3. Texture pole figures of the PTCa phase obtained by the analysis. Recalculated using (a) the harmonic method, linear scale (cause of the negative values), (b) WIMV, log scale, (c) E-WIMV, log scale. (d) Extracted experimental pole figures also in log scale, limited in the maximum χ angle due to the experiment. All using equal area projection.

reproduce them correctly and E-WIMV gives the best results. Table 1 reports the structure refinement results for the PTCa film confirming that the atomic positions of the compound were unaltered by the film deposition and agreed well with the equivalent in composition bulk compound.

The Ca fully stabilized zirconia film has been analyzed using both a texture (E-WIMV) and a residual stress model, as in this case the large shifts in the peaks position were due to the elastic strain resulting from the in-plane compressive residual stress. Fig. 5 shows the experimental and fitted spectra where these shifts are visible. By a careful check, it is possible to recognize that the shifts are not following the linear $\sin^2 \varphi$ and it is due to the strong texture. The BulkPathGEO method briefly outlined in the theory section was used for the modeling and was able to reproduce very well the non-linear trend. From the analysis the residual stress resulted to be isotropic and compressive in the film plane. The value refined by the program was indeed quite high and equal to $-3.47(5)$ GPa. Using a pure Reuss model the compressive stress was even higher to -3.6 GPa. The reconstructed pole figures for the zirconia film are reported in Fig. 6 and shows also in this case a nearly fiber texture quite common with the magnetron sputtering deposition technique.

For the last sample, the very thin zirconia film, both the reflectivity as well as some diffraction patterns were collected. We will analyze here only the result of the reflectivity measurement as for the diffraction case the film was too thin and gave only an amorphous like diffraction spectrum. The fitting result by MAUD is shown in Fig. 7 along with the electron density profile in Fig. 8. From the density profile and merging the simple three-layer model reported in Table 2 we can compute a total film thickness of 19.6 nm that nearly correspond to the expected 20 nm from the deposition process. From the table we may note a high roughness of the middle zirconia layer. This corresponds to the small density gradient visible in Fig. 8.

5. Conclusions

We have shown in this work that an integrated analysis approach can successfully analyze thin films

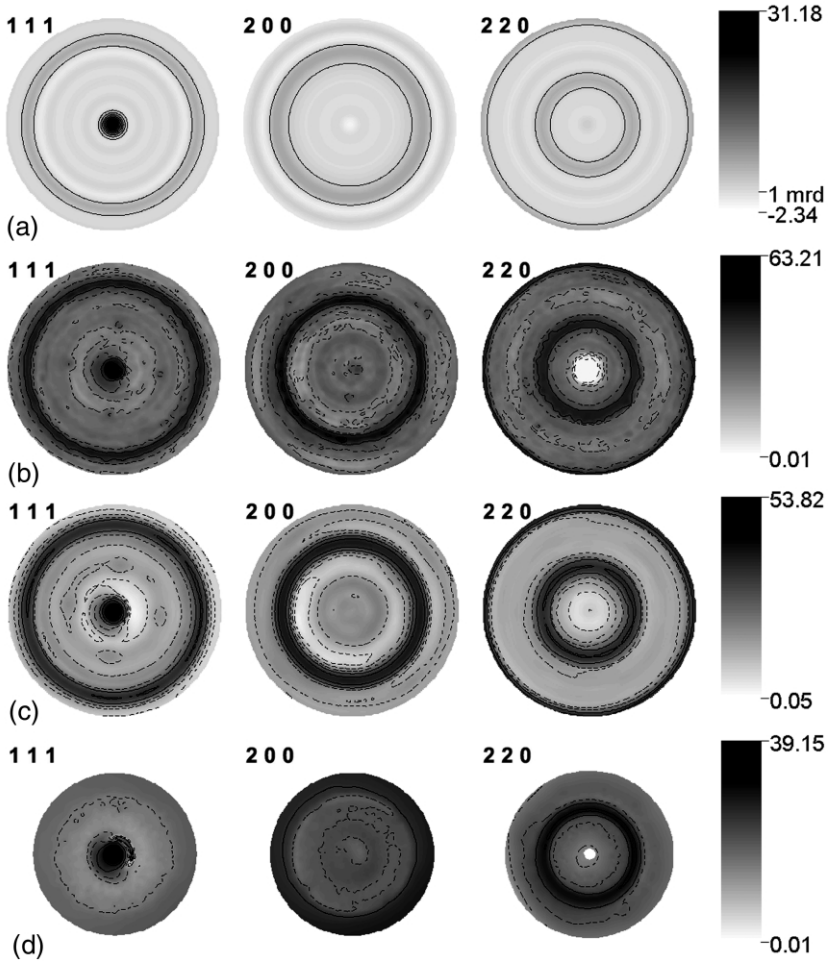

Fig. 4. Same pole figures as in Fig. 3 but for the Pt film. Recalculated from (a) harmonic, linear scale, (b) WIMV, (c) E-WIMV, both log scale. Experimental pole figures in (d), log scale.

and obtains quantitative results in term of texture, residual stresses, crystal structure and film structure. The result was obtained through the implementation of some new methodologies in a custom software package and a dedicated custom instrument for diffraction/reflectivity. Using the instrumentation and methodology here enlightened researchers can have powerful tools for a complete characterization of their samples for a correlation with the performance and properties of the films. The method applies also to multiphase/multilayered

Table 1
Structure refinement of the PTCa phase

Composition	$Pb_{0.76}Ca_{0.24}TiO_3$
Symmetry and space group	Tetragonal, P4mm
a (nm)	0.39234(1)
c (nm)	0.40574(1)
Pb, Ca	0, 0, 0
Ti	1/2, 1/2, 0.1919(8)
O	0, 1/2, 0.6137(7)

Cell parameters and fractional atomic positions. Estimated standard deviations (E.s.d.) in parenthesis corresponding to the last digit.

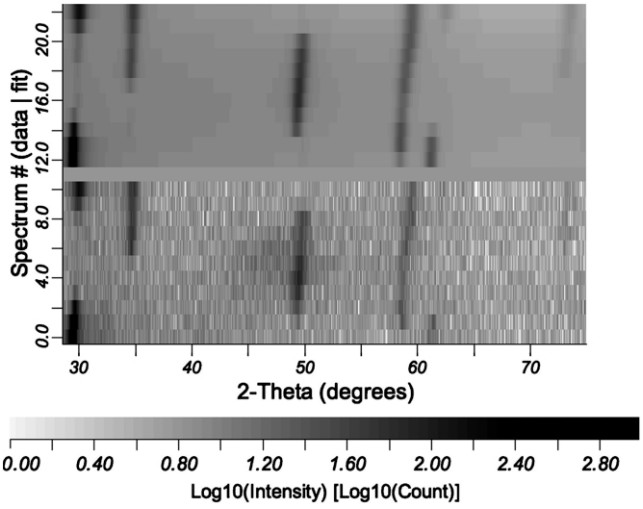

Fig. 5. Plot of the experimental and reconstructed spectra for the Ca stabilized zirconia film. The shift of the diffraction lines is due to the residual stress field. See text for details.

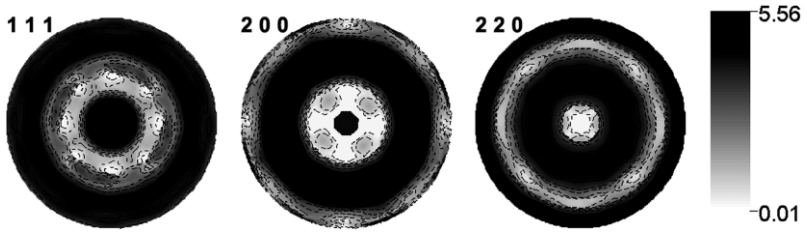

Fig. 6. Recalculated pole figures of the Ca–ZrO_2 phase corresponding to the analysis of Fig. 5.

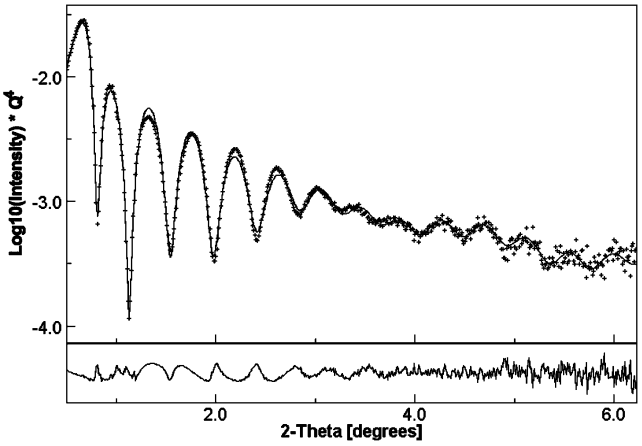

Fig. 7. Fitting of the reflectivity pattern for the zirconia thin film. Cross points correspond to experimental intensity. The continuous line represents the fit and the lower box contains the residual (difference between experimental and recalculated pattern).

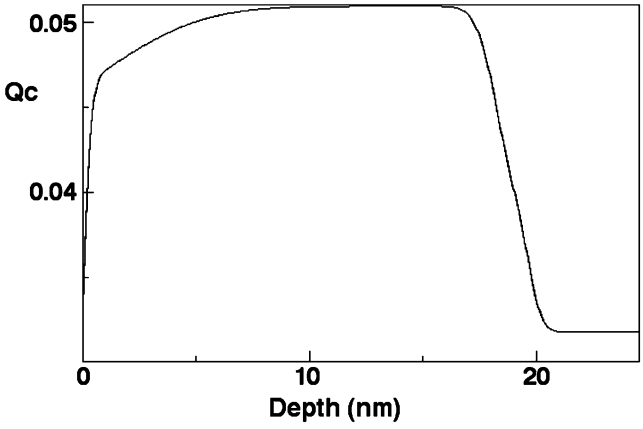

Fig. 8. Critical Q_c plot (proportional to the square of the electron density, see Appendix A) in $(e^-/Å^3)^{-1/2}$ vs. depth starting from the surface of the sample. The flat line after 20 nm corresponds to the Si substrate.

films where the previous methods fail due to strong peak overlapping.

Acknowledgments

The authors would like to thank S. Matthies for providing the routines for the BulkPathGEO method and C. Wiemer for the measurement of the SBT diffraction spectra and zirconia thin film reflectivity pattern. The work was sponsored and realized entirely inside the ESQUI European Project, contract number: G6RD-CT-1999-00169.

Appendix A:

I_i^{calc}	Calculated intensity of the spectrum at the point i
bkg_i	Polynomial background for the spectrum at the point i
I_0	Incident beam intensity
$L_p(2\theta_i)$	Lorentz-polarization factor at the 2θ point i
$A_i(\chi, \phi)$	Absorption factor at the point i for a sample orientation (χ, ϕ)
f_n	Volume fraction of phase n
$m_{k;n}$	Multiplicity of the diffraction plane k of phase n
$F_{k;n}$	Structure factor of the diffraction plane k of phase n
$S_{k;n}(x)$	Profile shape function of reflection k for phase n for a generic coordinate x
$2\theta_i$	Diffraction angle coordinate of point i

Table 2
Results of reflectivity analysis on the ZrO_2 thin film using the matrix formalism

Layer	Thickness (nm)	Q_c ($\sqrt{(e^-/Å^3)}$)	Roughness (nm)
Air	–	0	–
Cap layer	0.93(2)	0.043(1)	0.33(1)
Zirconia	17.5(2)	0.051(1)	3.5(1)
Intermediate layer	1.21(6)	0.037(3)	0.8(1)
Substrate (Si)	–	0.0317	0.5(1)

$2\theta_{k;n}$	Diffraction angle of reflection k for phase n
$P_{k;n}(\chi, \phi)$	Texture pole figure factor for reflection k for phase n at the sample orientation (χ, ϕ)
χ, ϕ	Azimuthal and polar angles in a polar coordinates
ODF(g)	Orientation distribution function in the Euler angles (g) representation
Q_c	Critical density, $Q_c = 0.03751\ \sqrt{\rho_e}$
ρ_e	Electron density

References

[1] H.M. Rietveld, Acta Cryst. 22 (1967) 151.
[2] R.A. Young, The Rietveld Method, IUCr, Oxford University Press, Oxford, UK, 1993.
[3] L. Lutterotti, P. Scardi, A. Tomasi, Mater. Sci. Forum 133–136 (1993) 57.
[4] H.J. Bunge, Texture Analysis in Material Science, Butterworths, London, 1982.
[5] N.C. Popa, J. Appl. Cryst. 25 (1992) 611.
[6] S. Matthies, G.W. Vinel, K. Helming, Standard Distribution in Texture Analysis, Akademie-Verlag, Berlin FRG, 1987.
[7] S. Matthies, L. Lutterotti, H.-R. Wenk, J. Appl. Cryst. 30 (1997) 31.
[8] H.-R. Wenk, K. Pawlik, J. Pospiech, J.S. Kallend, Textures Microstruct. 22 (1994) 233.
[9] H. Schaeben, J. Appl. Phys. 69 (3) (1991) 1320.
[10] M. Ferrari, L. Lutterotti, J. Appl. Phys. 76 (11) (1994) 7246.
[11] I.C. Noyan, J.B. Cohen, Residual Stress—Measurement by Diffraction and Interpretation, Springer, New York, 1987.
[12] S. Matthies, H.G. Priesmeyer, M.R. Daymond, J. Appl. Cryst. 34 (2001) 585.
[13] S. Matthies, M. Humbert, J. Appl. Cryst. 28 (1995) 254.
[14] J. Daillant, A. Gibaud, X-ray and Neutron Reflectivity: Principles and Applications, Springer, Berlin, 1999.
[15] Program MAUD. Available from: http://www.ing.unitn.it/~luttero/maud.
[16] ESQUI European Project. Available at: http://www.ing.unitn.it/~maud/esqui.